

Potential influence of the November–December Southern Hemisphere annular mode on the East Asian winter precipitation: a new mechanism

Zhiwei Wu · Juan Dou · Hai Lin

Received: 29 September 2013 / Accepted: 2 July 2014 / Published online: 20 July 2014
© Springer-Verlag Berlin Heidelberg 2014

Abstract As the leading mode of the global atmospheric mass inter-annual variability, the Southern Hemisphere annular mode (SAM) may exert potential influences to the Northern Hemisphere (NH) climate, but the related physical mechanism is not yet clear. In this study, it is found that the November–December (ND) SAM exhibits a significant inverse relationship with the winter precipitation over East Asia, particularly southern China. Observational and numerical evidences show that anomalous ND SAM is usually associated with a South Atlantic–Pacific dipole sea surface temperature anomaly (SSTA) which persists into ensuing winter. The dipole SSTA can modulate the variability of the Inter-tropical Convergence Zone (ITCZ) in Pacific. Subsequently, a distinguished atmospheric teleconnection pattern is induced and prevails over the NH mid-latitude region as a response to the anomalous ITCZ. Large areas of high pressure anomalies are triggered at upper troposphere over East Asia and centered over southern China, which favors less precipitation over East Asia, particularly southern China, and vice versa. Through such a physical mechanism, the notable influence of the ND SAM can sustain through the following season and impact on the NH winter climate.

Keywords Southern Hemisphere annular mode · Northern Hemisphere climate · Mechanism

1 Introduction

The Southern Hemisphere (SH) annular mode (SAM) is a seesaw phenomenon between the sea level high pressure belt across Chile and Argentina and the low pressure area of Weddell Sea and the Bellingshausen Sea (Walker 1928; Kidson 1975; Rogers and van Loon 1982; Cai et al. 1999; Thompson and Wallace 2000a, b; Cai and Watterson 2002). Trenberth et al. (2005) investigated the interannual variability of patterns of global atmospheric mass and found that the dominant global monthly variability overall is associated with the SAM. Previous studies confirmed that the SAM has great influences on the SH climate, i.e., Australian and South Africa rainfall, anomalously dry conditions over southern South America, New Zealand and Southern Australia, and Antarctic sea ice (e.g., Li et al. 2005; Gillett et al. 2006; Hendon et al. 2007; Yuan and Li 2008; Kidson et al. 2009; Li and Smith 2009; Sun and Li 2012; and many others). Although the influence of the SAM on regional climate such as Southwest Western Australia winter rainfall is in debate (Feng et al. 2010; Cai et al. 2011), the SAM is probably the most important pattern of climate variability in the SH middle and high latitudes.

Climate impacts of the SAM may be not limited in the SH. Some studies already suggested that the SAM anomalies might be related to some anomalous climate events in the Northern Hemisphere (NH). For instance, Nan and Li (2003) found that there is a significant positive correlation between the boreal spring SAM and the following summer monsoon rainfall in the middle and lower reaches of the Yangtze River. Wu et al. (2009a) revealed that the boreal

Z. Wu (✉) · J. Dou
Earth System Modeling Center, Key Laboratory
of Meteorological Disaster of Ministry of Education,
Nanjing University of Information Science and Technology,
Nanjing 210044, Jiangsu, China
e-mail: wzw.lasg@gmail.com; zhiweiwu@nuist.edu.cn

H. Lin
Atmospheric Numerical Weather Prediction Research Section,
Environment Canada, Dorval, QC H9P 1J3, Canada

autumn SAM exhibits an intimate linkage with the China winter monsoon variability. Zheng and Li (2012) found that the boreal winter SAM is significantly correlated with spring precipitation over South China. Although the above linkages between the SAM and regional climate in the NH are statistically significant, a crucial issue is how the SAM signals propagate from the SH into the NH and in turn affect the NH climate.

Some physical mechanisms are proposed to interpret such cross-equatorial impacts of the SAM. For instance, Thomas and Webster (1994) suggested that cross-equatorial wave propagation from the SH into the NH will most likely be observed when the westerly duct is open. In light of the intimate connection between the ENSO and SAM variability, ENSO might be an implicit link between the SAM and NH climate (L'Heureux and Thompson 2006). Indian Ocean circulation change was proposed to play a “bridge” role in transmitting the SAM influence into the NH (Nan et al. 2008). Observational and numerical evidences provided by Wu et al. (2009a) and Zheng and Li (2012) showed that the anomalous SAM is usually associated with a hemispheric-scale sea surface temperature (SST) anomaly (SSTA) belt in the region (45°S–30°S). The latter can affect the strength of the Hadley cell and in turn modulate the NH climate. Nevertheless, physical mechanisms on how the SAM influence crosses the equator into the NH remain controversial and are far from being well understood.

Another issue is that since the SAM owns its existence to internal atmospheric dynamics in the middle latitudes (Thompson and Wallace 2000a, b), it lacks the mechanism to generate persistent or predictable variations (Wu et al. 2009b, 2012; Xu et al. 2013; Yin et al. 2013), and potential predictability of such fluctuations can only arise from low boundary forcing such as SSTAs (Charney and Shukla 1981; Shukla 1998; Li and Wu 2012). It is not yet clear whether the SAM effect can persist through the following season. If so, what roles do SSTAs play in “memorizing” the SAM signal?

This study attempts to answer the above questions. The manuscript is structured as follows. Section 2 describes the datasets, model and methodology used in this study. Section 3 presents the observed relationship between the November–December (ND) SAM and East Asian winter (December–January–February, DJF) precipitation. In Sect. 4, a new physical mechanism is proposed to interpret the ocean roles in “prolonging” the SAM effect from late autumn through winter and how the SAM influence crosses the equator and reaches the NH climate. Numerical experiments are performed with a simple general circulation model (SGCM) to further confirm the new physical mechanism proposed in Sect. 5. The last section summarizes major findings and some outstanding issues.

2 Data, model and methodology

The major datasets used in this work include: (1) monthly precipitation data from the global land precipitation (PREC/L) data for the 1979–2012 period gridded at $1.0^\circ \times 1.0^\circ$ resolution (Chen et al., 2002) and from CMAP (Xie and Arkin 1997) (1979–2010), respectively; (2) monthly circulation data, gridded at $1.5^\circ \times 1.5^\circ$ resolution, taken from the European Centre for Medium-Range Weather Forecasts (ECMWF) Re-Analysis interim dataset (ERA-interim) for the period 1979–2012 (Dee et al. 2011); (3) monthly SST data from the improved Extended Reconstructed SST Version 3 (ERSST V3; Smith et al. 2008) (1979–2012); (4) monthly SAM index (SAMI) defined by Marshall (2003) and Nan and Li (2003) (1979–2012). In this study, autumn and winter all refer to boreal seasons.

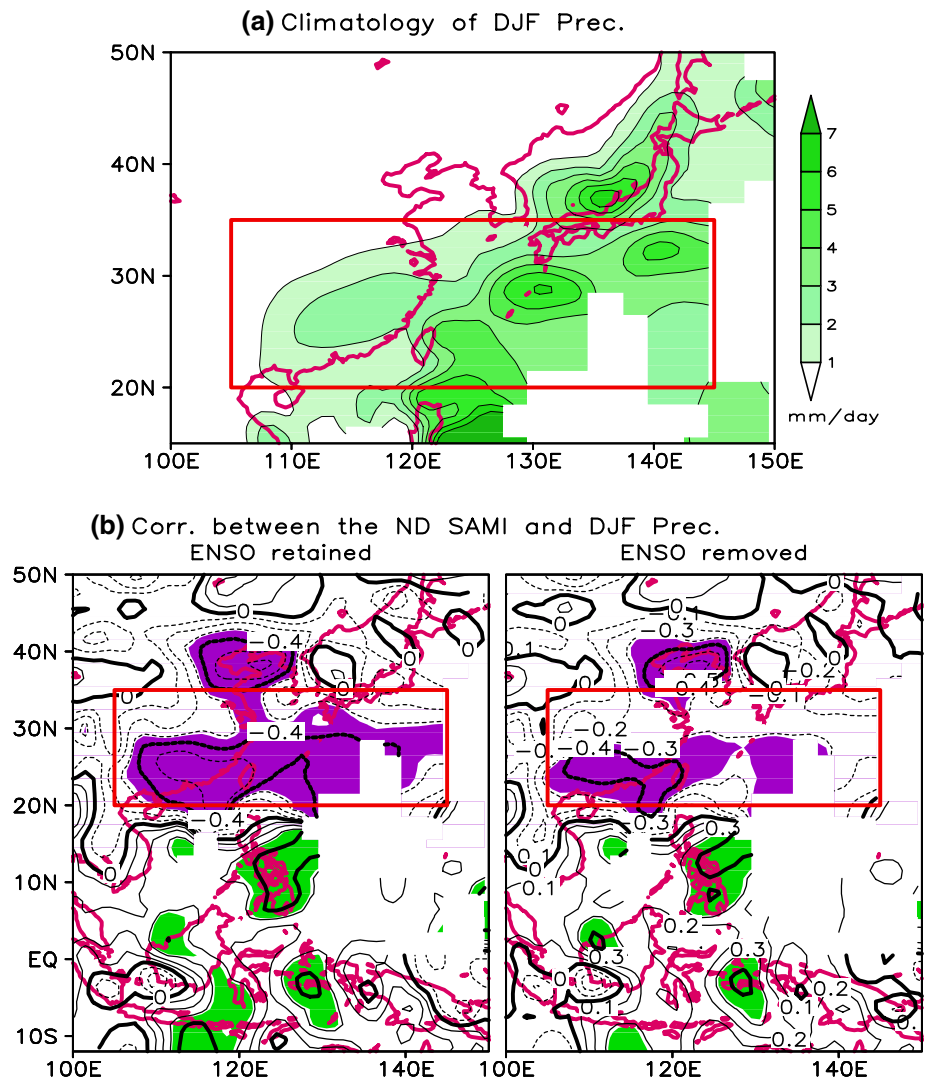
All the numerical experiments presented in this paper are based on a dry spectral primitive equation model first developed by Hoskins and Simmons (1975). The resolution used here is triangular 31, with 10 equally spaced sigma levels (Wu et al. 2009b). An important feature of this model is that it uses a time-averaged forcing calculated empirically from observed daily data. Due to its simplicity in physics, it is referred to as a “simple general circulation model (SGCM).” This model is able to reproduce remarkably realistic stationary planetary waves and the broad climatological characteristics of the transients are in general agreement with observations (Hall 2000). The advantage of this SGCM model is that dynamical mechanisms are more easily isolated.

To derive the dominant coupling mode between ND circulation anomalies over the SH mid-high latitudes and DJF precipitation in East Asia, we use the singular value decomposition (SVD) technique (Bretherton et al. 1992). The SVD analysis is conducted from the covariance between ND sea level pressure (SLP) in the SH region (0° – 360° , 90° S– 30° S) and PREC/L precipitation anomalies over East Asia (100° E– 150° E, 15° N– 50° N) in the 34 winters from 1979 through 2012.

3 East Asian winter precipitation and the ND SAM

Figure 1a presents the winter climatology of precipitation over East Asia for the period 1979–2012. The major winter rainfall areas in East Asia are basically located over southern China and the oceanic areas from Japan to Philippine. Overlapped with these climatological precipitation centers (red box in Fig. 1a), large areas of significant negative correlation between the ND SAM and the DJF precipitation control the southern China and expand eastward towards the oceanic areas south of Japan (red box in the left panel of Fig. 1b), whereas significant positive correlation over

Fig. 1 **a** Long-term average (color shadings) of the precipitation rate during boreal winter (December–January–February, DJF) over East Asia for the period 1979–2012. The unit of the precipitation is mm day^{-1} . The data used is PREC/L precipitation data. **b** *Left panel* The correlation pattern between the November–December (ND) Southern Hemisphere (SH) annular mode index (SAMI) and DJF precipitation rate; *Right panel* Same as the left panel, but for the partial correlation patterns with the DJF ENSO signal removed. The contour interval is 0.1. The green shadings in Fig. 1b denote positive correlation coefficients exceeding 95 % confidence level based on the Student *t* test, purple negative. The precipitation rate averaged in the red box (105°E – 145°E , 20°N – 35°N) is defined as a rainfall index (RI)



the Maritime Continent. This indicates that a strong SAM ND is usually followed by a less-precipitation winter over East Asia and a rich-precipitation winter over the Maritime Continent, and vice versa. To verify whether the correlation between the ND SAMI and the DJF precipitation depends on ENSO influence or not, the partial-correlation approach is used to remove the DJF ENSO signal. The correlation between the ND SAM and the DJF precipitation remains significant over southern China (red box in the right panel of Fig. 1b). To quantitatively measure the strength of the DJF precipitation over East Asia, a rainfall index (RI) is defined as the averaged precipitation within the domain (105°E – 145°E , 20°N – 35°N) (red box in Fig. 1).

To further elaborate the relationship between the ND circulation anomalies over the SH mid-high latitudes and winter rainfall anomalies over East Asia, Fig. 2 presents the first SVD mode of ND SLP in the SH (0° – 360° , 90°S – 30°S) and DJF precipitation anomalies over East Asia (100°E – 150°E , 15°N – 50°N). This leading mode accounts

for 73.9 % (above the noise level) of the total squared covariance. The SH SLP pattern is characterized by a seesaw pattern with a significant negative center over the Antarctic continent and an evident circum-global positive belt in the middle latitudes (left panels in Fig. 2a, b). This pattern reflects a typical positive SAM phase as documented by Thompson and Wallace (2000a, b). The corresponding precipitation pattern basically shows a mono-sign pattern over the East Asian middle latitudes. A strong negative correlation center dominates over southern China extending eastward to the oceanic areas south of Japan (right panels in Fig. 2a, b). This result is consistent with the conclusion from Fig. 1b and further confirms the significant inverse relationship between the ND SAM and winter precipitation over East Asia.

Figure 3a shows the time series of the ND SAMI and the DJF RI for the period 1979–2012 and no obvious increasing or decreasing trend can be detected with them. They are basically dominated by the inter-annual variations and

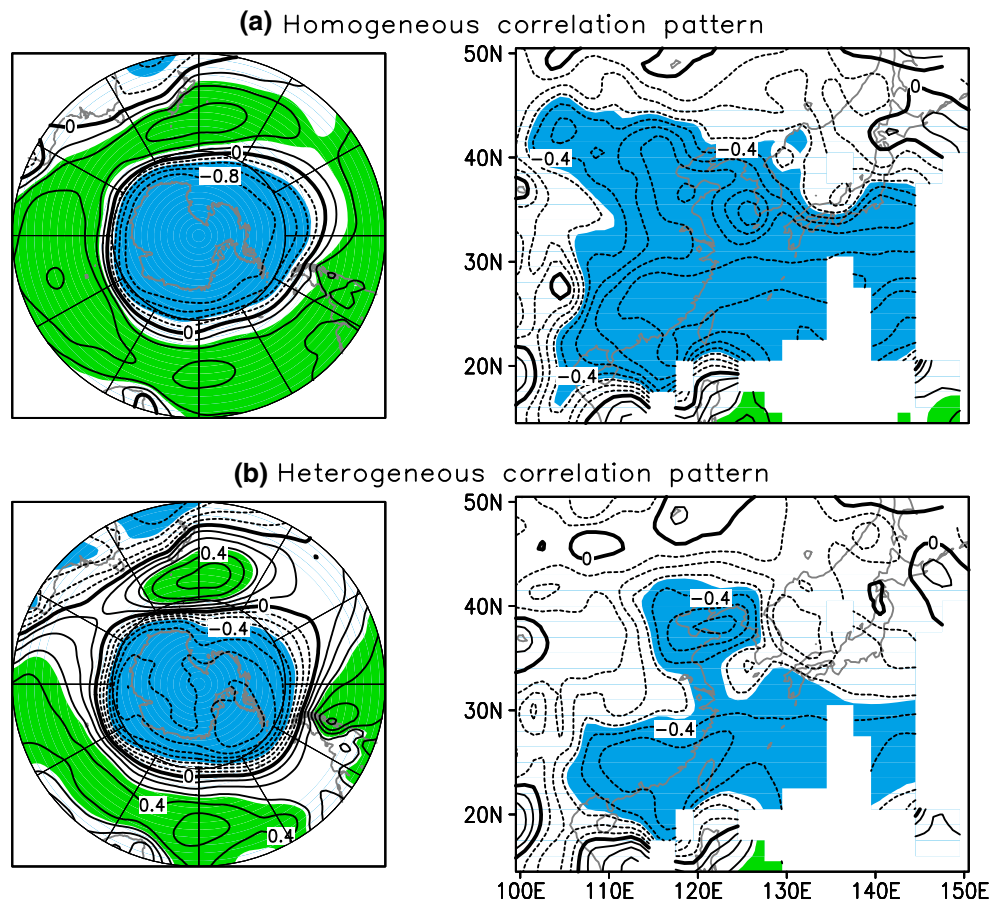


Fig. 2 The leading SVD mode for the ND sea level pressure (SLP) anomalies (*left panels*) over the SH (0° – 360° , 30° S– 90° S) and the DJF precipitation rate anomalies (*right panels*) over East Asia. The *upper panels* are the **a** homogeneous correlation patterns, and the lower ones the **b** heterogeneous correlation patterns. The areas with

positive correlation coefficients being significant at the 95 % confidence level are shaded *green*, *negative blue*. The temporal correlation coefficient between the corresponding expansion coefficients is 0.69, which is significant above 99 % confidence level based on the Student *t* test. The contour interval is 0.1

exhibit a significant out-of-phase relationship. Their correlation coefficient reaches -0.55 , exceeding the 95 % confidence level based on the Student *t* test. An interesting phenomenon is that such a significant correlation with the DJF RI only exists in the November and December SAMI (Fig. 3b). Another SAMI defined by Nan and Li (2003) is used to further verify the above conclusion and the result is just the same (not shown). This may be interpreted by the chaotic nature of the atmosphere (or the SAM), namely, the SAM itself is lack of persistence (Lorenz 1963; Wu et al. 2009b). Then, how can the ND SAM affect the winter rainfall over East Asia?

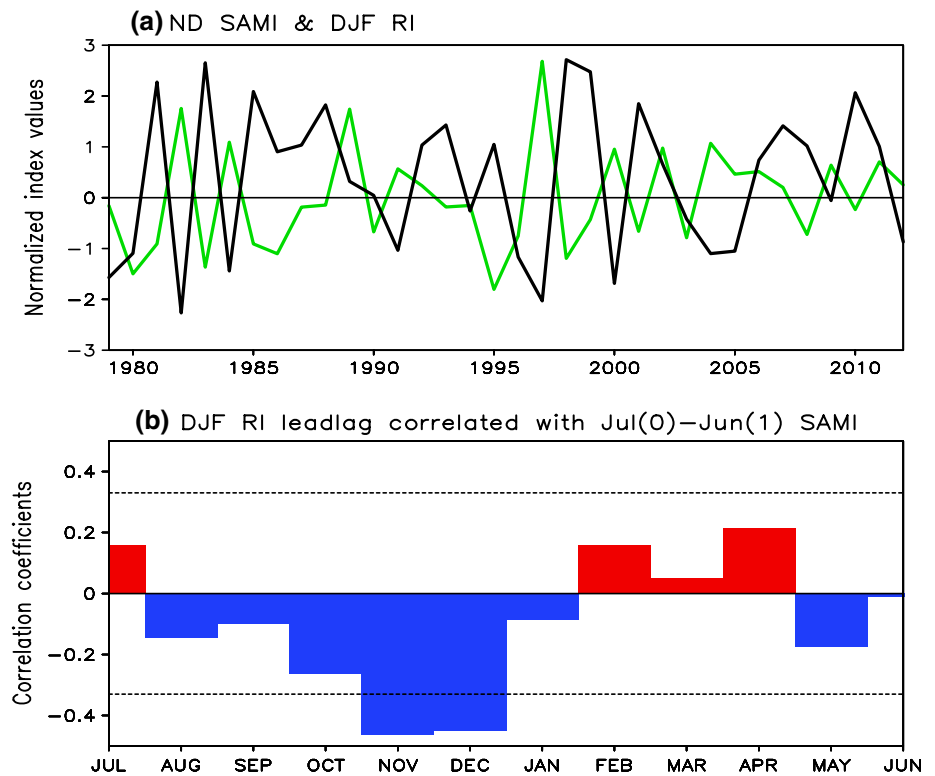
4 Physical mechanisms

It is generally recognized that the predictable variations of atmosphere can only arise from coupled mechanisms that involve low boundary forcing such as SSTA (Charney and

Shukla 1981; Shukla 1998; Lin and Wu 2011). In light of this, SSTA might provide an effective way to “prolong” the SAM influence through interactions between the atmosphere and the more slowly varying oceans.

We examined the regressed SST patterns from late autumn through winter to the ND SAMI, respectively (Fig. 4). A prominent feature is that associated with the anomalous ND SAM, a notable dipole SSTA pattern emerges in the South Atlantic-Pacific areas and persists from ND through January–February (JF). To quantitatively depict such a dipole SSTA pattern during winter, a simple South Atlantic-Pacific dipole (SAPD) index is defined as difference between averaged SST in the blue and red boxed oceanic areas (blue minus red) (Fig. 4). The SAPD index time series exhibit a highly consistent variability with the ND SAMI, their correlation coefficient reaching 0.67 beyond 99.9 % confidence level based on the Student *t* test. Such a consistency allows us to interpret it as the ocean “memory” effect to the ND SAM signal. Another

Fig. 3 **a** Time series of the ND SAMI (black curve) and the DJF RI (green curve) for the period of 1979–2012. The correlation coefficient between them is -0.55 , exceeding the 95 % confidence level based on the Student t test. **b** Lead-lag correlations (color bars) between the DJF RI and the SAMI from July(0) through June(1). “0” denotes the simultaneous year and “1” the following year. The two dashed horizontal lines represent the 95 % confidence level



Regression between the ND SAMI and

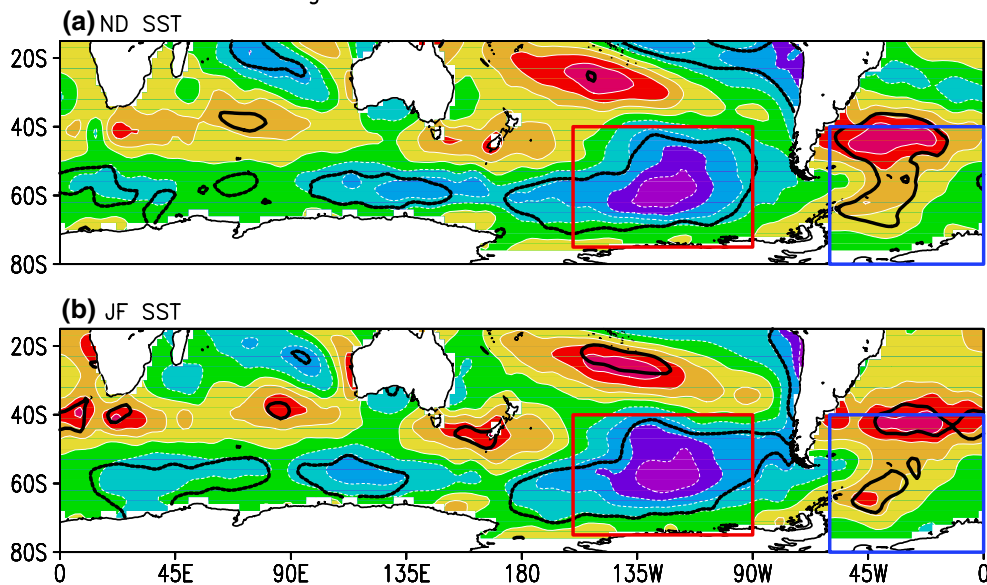


Fig. 4 **a** ND and **b** January–February (JF) sea surface temperature (SST) regressed against the ND SAMI. The shading interval is 0.05 K. The SST anomalies included in the bold black curves exceed the 95 % confidence level based on the Student t test. A South Atlan-

tic–Pacific dipole (SAPD) index is defined by the SST difference in the blue and red boxes (blue minus red). The blue box denotes the South Atlantic domain (80°S–40°S, 0°–60°W), while the red box represents the South Pacific (75°S–40°S, 90°W–160°W)

interesting feature is that a tripole SSTA pattern exists in the SH Indian Ocean, yet with a weak amplitude and lack of significant persistence. Therefore, we will not focus on

this tripole SSTA in this study (see the last section). Then, what influences may such SAPD SSTA have on the large-scale atmospheric circulation?

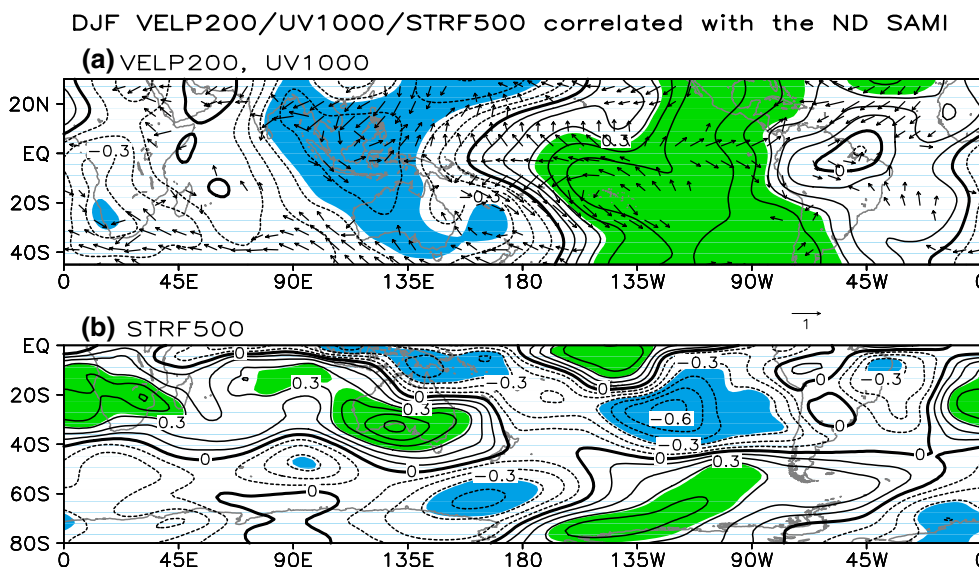


Fig. 5 Correlation patterns between the ND SAMI and DJF **a** 200 hPa velocity potential (VELP200, contours), 1,000 hPa winds (UV1000, vectors) and **b** 500 hPa stream function (STRF500) (contours). The contour interval is 0.1. The wind vectors plotted exceed

the 95 % based on the Student *t* test. The green shadings denote positive correlation coefficients exceeding 95 % confidence level, blue negative

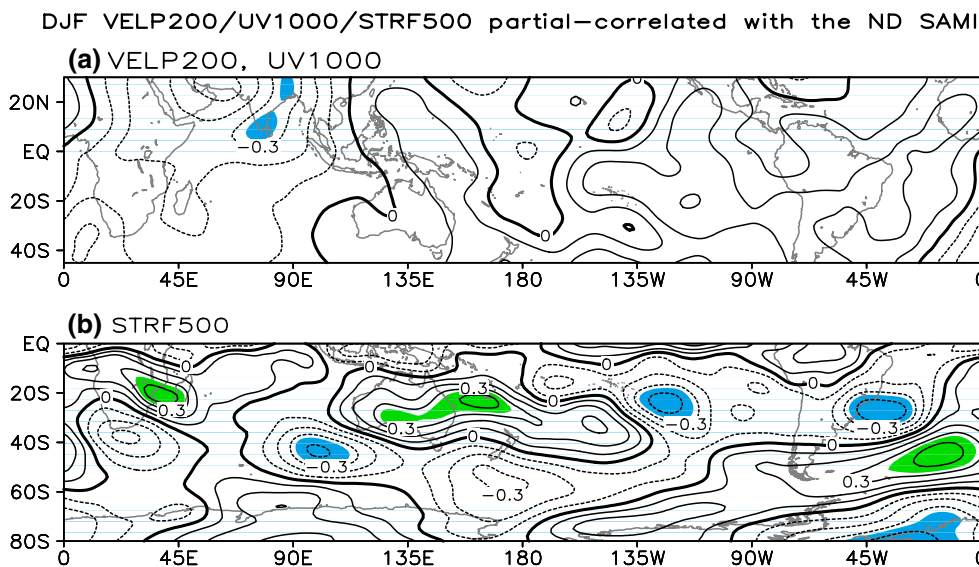


Fig. 6 Same as Fig. 5, but for the partial correlation patterns with the DJF SAPD signal removed

Before answering the above question, we need to clarify the dynamic structures of the DJF circulation anomalies associated with the anomalous ND SAM. Figure 5a displays 200 hPa velocity potential (VELP200) and 1,000 hPa wind anomalies regressed to the ND SAMI. An evident feature of VELP200 is that significant negative correlations prevail over the low-latitude region from the Maritime Continent to Australia. Meanwhile,

anomalous wind convergence controls the Maritime Continent at 1,000 hPa, with westerly wind anomalies over the equatorial eastern Indian Ocean and easterly wind anomalies over the equatorial western Pacific. Over the tropical central-eastern Pacific, the situation is just opposite. These indicate that a strong ND SAM usually provides a precursory condition for the intensified DJF Walker Circulation.

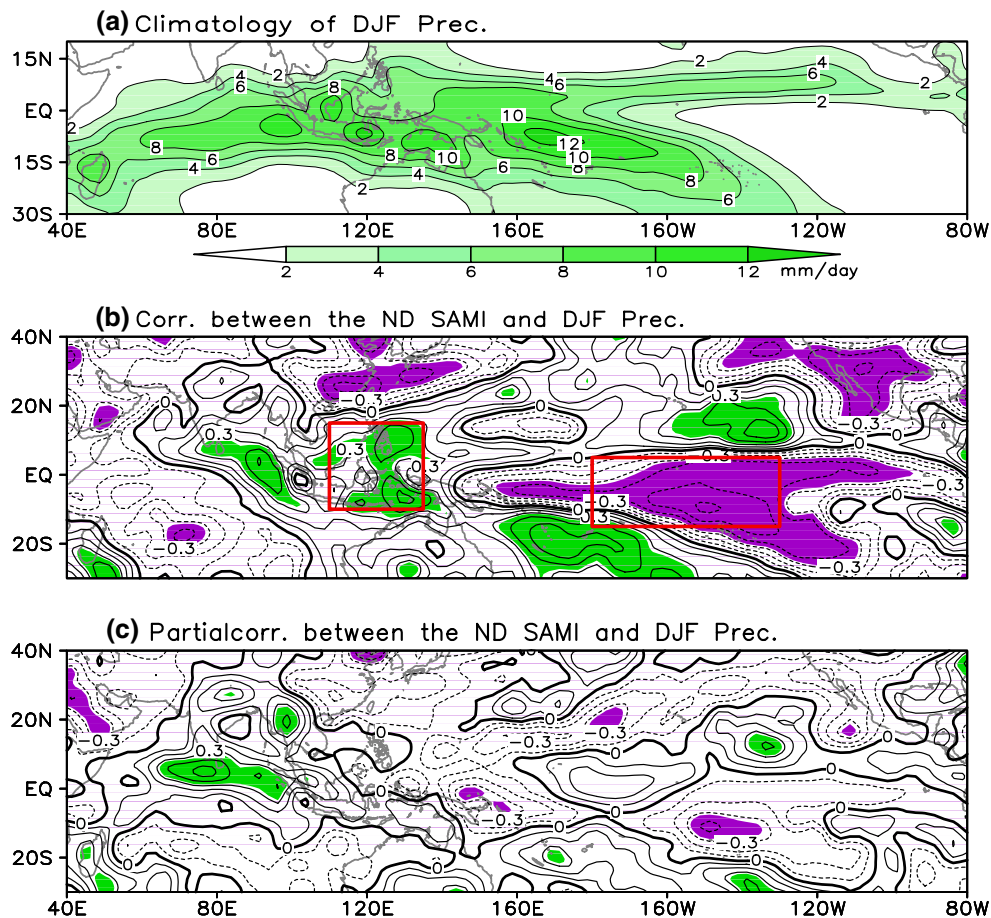


Fig. 7 **a** Long-term average (*color shadings*) of the DJF precipitation rate over East Asia for the period 1979–2010. The unit of the precipitation is mm day^{-1} . The data used is CMAP precipitation. **b** The correlation pattern between the ND SAMI and DJF precipitation rate. The contour interval is 0.1. An Inter-tropical Convergence Zone index (ITCZI) is defined by the averaged precipitation rate difference

in the western ($10^{\circ}\text{S}–15^{\circ}\text{N}$, $110^{\circ}\text{E}–135^{\circ}\text{E}$) and eastern ($15^{\circ}\text{S}–5^{\circ}\text{N}$, $180^{\circ}–130^{\circ}\text{W}$) boxes (western minus eastern). **c** Same as Fig. 7b, but for the partial correlation with the DJF SAPD SSTA signal removed. The *green shadings* in Fig. 7b, c denote positive correlation coefficients exceeding 95 % confidence level based on the Student *t* test, *purple* negative

Another notable feature of the DJF circulation anomalies is that 500 hPa stream function (STRF500) field exhibits noticeable wave train patterns propagating from the high latitudes towards the tropics (Fig. 5b). The amplitude of the STRF500 wave train decreases northeastward along the latitude, with the maximum loading center above the SAPD area. These imply that the origin of the wave train may be from the SAPD SSTA.

An interesting phenomenon is that if the partial-correlation approach is used to remove the DJF SAPD signal, the intensified Walker Circulation in Fig. 5a becomes unobvious over the local region (Fig. 6a). Similar feature also exists in Fig. 6b: the STRF500 wave train pattern becomes unclear with the SAPD signal removed, compared with Fig. 5b. These indicate that the SAPD SSTA pattern may play a crucial “ocean bridge” role in linking the ND SAM with the DJF circulation anomalies over the Indo-Pacific region.

The most important question is how the influence of the SAM can cross equator and reach the NH. We investigated the changes in the Pacific Inter-tropical Convergence Zone (ITCZ) associated with the anomalous SAM (Fig. 7). It can be easily discerned that in the climatological ITCZ rainfall belt (Fig. 7a), a dipole correlation pattern exists, with significant positive correlation in the Maritime Continent and negative correlation in the equatorial central-eastern Pacific (Fig. 7b). It indicates that a strong ND SAM is usually followed by intensified winter precipitation over the Maritime Continent and suppressed precipitation over the equatorial central-eastern Pacific, and vice versa. Meanwhile, significant negative correlation prevails over East Asia (Fig. 7b). We compared the partial-correlation pattern in Fig. 7c. If the DJF SAPD signal is removed, the dipole correlation pattern in the ITCZ disappears, so does the significant negative correlation over East Asia. This result is consistent with the conclusion from Fig. 6 that the SAPD SSTA

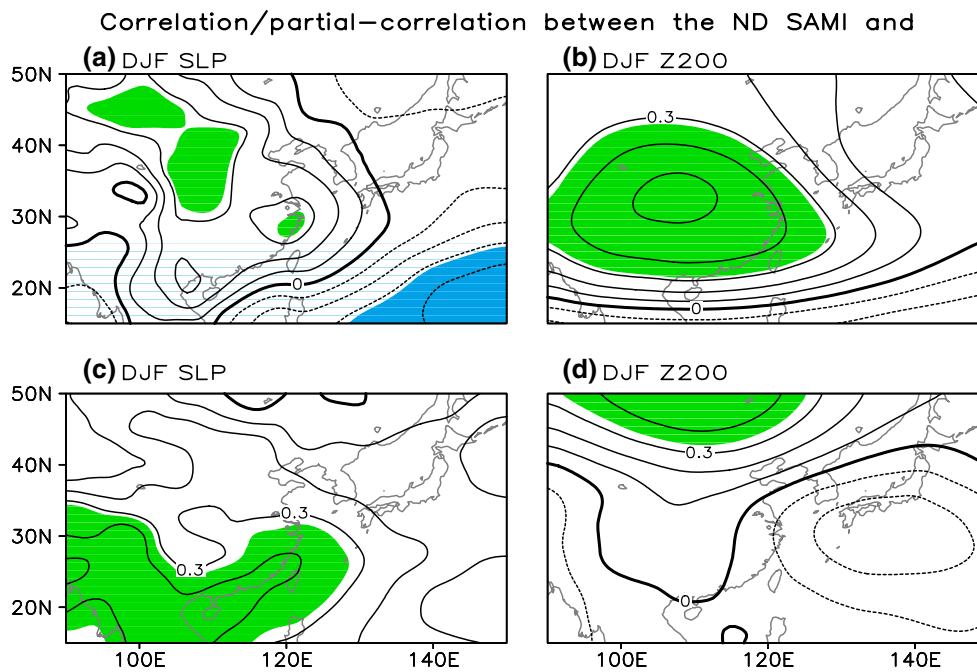


Fig. 8 Correlation patterns between the ND SAMI and DJF **a** SLP (contours) and **b** 200 hPa geo-potential height (Z200) (contours). The contour interval is 0.1. The green shadings denote positive correlation

coefficients exceeding 95 % confidence level based on the Student *t* test, blue negative. **c** and **d** same as **a** and **b**, but for the partial-correlation with the DJF ITCZI signal removed

pattern may play a crucial “bridge” role in the linkage between the ND SAM and the winter tropical circulation.

Changes in the Pacific ITCZ may lead to changes in the NH teleconnection pattern (e.g., He et al. 2011). To quantify the interannual variations of the ITCZ dipole anomaly, an ITCZ index (ITCZI) is defined as the difference between averaged precipitation in the two boxed areas (west minus east boxes) (Fig. 7b). Figure 8 presents the correlation and partial-correlation patterns between the ND SAMI and the NH circulations in boreal winter. SLP in the tropical region basically exhibits a zonal seesaw pattern. During a positive SAMI phase, large areas of high SLP anomalies control the Siberia region and expand southeastward towards southern China. This indicates that the Siberian High is strengthened (Wu et al. 2011). In the meanwhile, positive 200 hPa geo-potential height (Z200) anomalies cover southern China and extend eastward towards the oceanic areas south of Japan Islands (Fig. 8b). Such circulation configurations may favor less winter rainfall in southern China (Fig. 9a). During a negative SAMI phase, the situation tends to be opposite.

In contrast, if the partial-correlation approach is used to remove the ITCZI signal, the intensified Siberian High in Fig. 8a becomes unobvious over the local region (Fig. 8c). Similar feature also exists in Fig. 8d: the positive Z200 anomalies and negative precipitation anomalies over southern China become unclear with the ITCZI signal removed, compared with Figs. 8b and 9b. These indicate that the

ITCZ may play a crucial “ocean bridge” role in linking the ND SAM with the DJF circulation and precipitation anomalies over East Asia.

According to the above analysis, the linkage among the ND SAM, the SAPD SST anomalies, the ITCZ and East Asian winter precipitation may be summarized as following: the ND SAM anomalies are usually associated with a SAPD pattern which can persist from late autumn through winter; such SAPD SST anomalies modify the ITCZ variability; the anomalous ITCZ may lead to the atmospheric teleconnection change in the NH, and in turn influences the precipitation variability over East Asia.

5 Numerical experiments

To further verify the above conclusions, two numerical experiments are conducted with the SGCM. One is the SAPD SSTA forcing experiment, the other the anomalous ITCZ forcing. The SAPD experimental design has been used to study the SH teleconnections of the SAPD SSTA, while the ITCZ experiment to study the NH teleconnections of the anomalous ITCZ.

To mimic the diabatic heating effects of a high SAPD forcing, we imposed one heating source and one cooling source; each has an elliptical squared cosine distribution in latitude and longitude (Fig. 10a). Mimicing a low SAPD forcing is the same as mimicing a high SAPD forcing

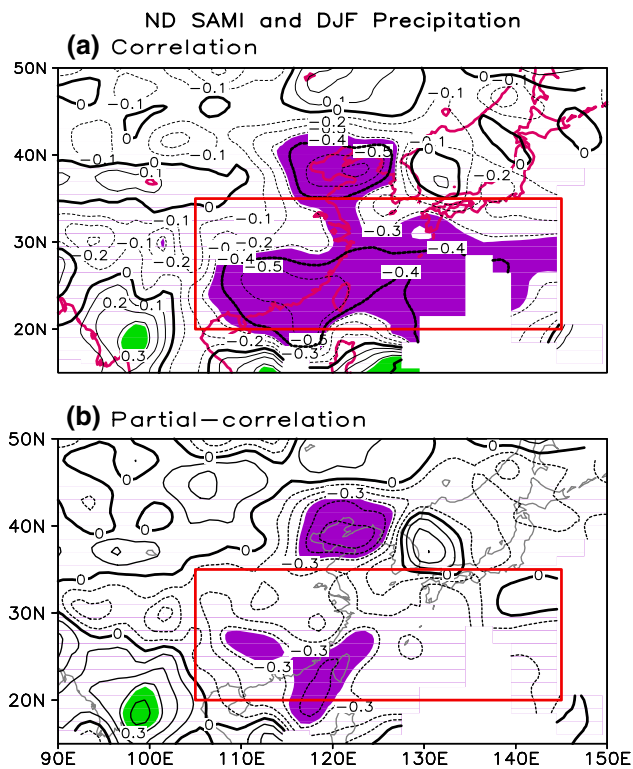


Fig. 9 **a** Correlation pattern between the ND SAMI and DJF precipitation rate over East Asia. The precipitation data is from PREC/L data. The contour interval is 0.1. The *green shadings* denote positive correlation coefficients exceeding 95 % confidence level based on the Student *t* test, *purple* negative. **b** same as **a**, but for the partial-correlation with the DJF ITCZI signal removed

except for a reversed sign. To mimic the diabatic heating effects of a high ITCZI forcing, one heating source and one cooling source are imposed (Fig. 11a). A low ITCZI forcing is the same as a high ITCZI forcing except for a reversed sign. Based on the previous work by Hoskins and Karoly (1981) and Wu et al. (2009b), the vertically integrated heating (or cooling) rate of the anomalous SAPD forcing imposed here is 0.5 K/day (approximately the latent heating rate released by an extra 2 mm precipitation per day), and that of the anomalous ITCZ 2.5 K/day (approximately the latent heating rate released by an extra 10 mm precipitation per day). The vertical heating profile of the SAPD is σ^4 , peaking at around 850 hPa, while that of the ITCZ is $(1-\sigma) \sin[\pi(1-\sigma)]$ and peaks around 300 hPa. Four perturbed experiments were integrated for 3,700 days. The last 3,600-day integrations were used to construct an ensemble (arithmetic) mean. Note that the result is not sensitive to the selection of initial condition, since the analysis is conducted for the period after the climate equilibrium is reached.

The model responses of stream function at 550 hPa (STRF550) to the anomalous SAPD forcing are shown in

Fig. 10b (high minus low SAPD). A pronounced wave train pattern is induced over the SH and propagates from the Weddell Sea towards the Maritime Continent. Large areas of negative velocity potential values at 250 hPa (VELP250) prevail over the tropical Indo-Pacific region, whereas positive values over the tropical Atlantic and eastern Pacific. It indicates that the Walker Circulation tends to be stronger and favors more precipitation over the Maritime Continent in a high SAPD winter. This experiment further confirms that the SAPD SSTA can affect the tropical atmospheric circulation and ITCZ variability through triggering an equatorward Rossby wave train in the SH. This numerical conclusion is primarily consistent with the partial-correlation results in Figs. 6 and 7c.

Figure 11 shows the SGCM responses of 250 hPa geopotential height (Z250) over the NH to the anomalous ITCZ forcing. The model responds an evident Z250 positive belt between 20°N and 40°N, centered over southern China and extending eastward to the central North Pacific. It means that Z250 over these areas are usually higher in a positive ITCZI winter, which favors less precipitation over the local region. For a negative ITCZI winter, the situation tends to be opposite. This may explain the correlation pattern between the winter ITCZI and precipitation (red box in Fig. 9).

To summarize, the primary response of the SH atmosphere to anomalous SAPD SSTA is an equatorward Rossby wave train propagating northeastward from the Weddell sea toward the Maritime Continent and modulating the tropical Walker Circulation and the ITCZ variability. Under the anomalous ITCZ forcing, the SGCM responds a distinct teleconnection pattern prevailing over the NH middle latitudes at the upper level, with high or low pressure anomalies centered over southern China.

6 Conclusion and discussion

Many studies have noticed the statistical linkage between the SAM and the NH climate (e.g., Nan and Li 2003; Wu et al. 2009a; Zheng and Li 2012; and others), yet the detailed physical mechanisms remain controversial (Thomas and Webster 1994; L'Heureux and Thompson 2006; Nan et al. 2008; Wu et al. 2009a). The main difficulty is how the SAM signals propagate from the SH into the NH and in turn affect the NH climate. Another issue is that due to lack of persistence, how the precursory SAM signals are “stored” and impact on the climate in the ensuing season.

In this study, we examined the observed relationship between the ND SAM and East Asian winter rainfall and found that the ND SAM has a significant inverse relationship with winter precipitation over East Asia, particularly southern China. Although the anomalous SAM signals decay

Fig. 10 **a** Vertically averaged anomalous heating rate for the SAPD forcing run. The contour interval is 0.1 K day^{-1} . **b** 550 hPa stream function (STRF550) responses. The contour interval is $2 \times 10^5 \text{ m}^2 \text{ s}^{-1}$. The *green shadings* represent those with a positive response over $4 \times 10^5 \text{ m}^2 \text{ s}^{-1}$, *purple* below $-4 \times 10^5 \text{ m}^2 \text{ s}^{-1}$. **c** 250 hPa velocity potential (VELP250) responses. The contour interval is $1 \times 10^5 \text{ m}^2 \text{ s}^{-1}$. The *green shadings* represent those with a positive response over $3 \times 10^5 \text{ m}^2 \text{ s}^{-1}$, *purple* below $-3 \times 10^5 \text{ m}^2 \text{ s}^{-1}$. Contours with negative values are dashed for **a**, **b** and **c**. The *bold contour* denotes zero, while the zero contour for **a** is omitted

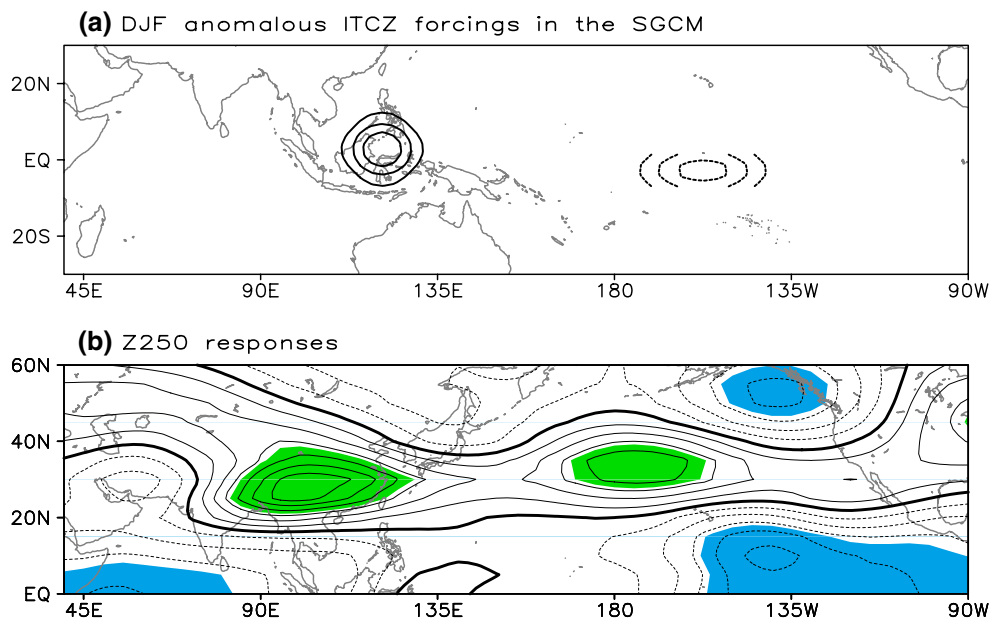
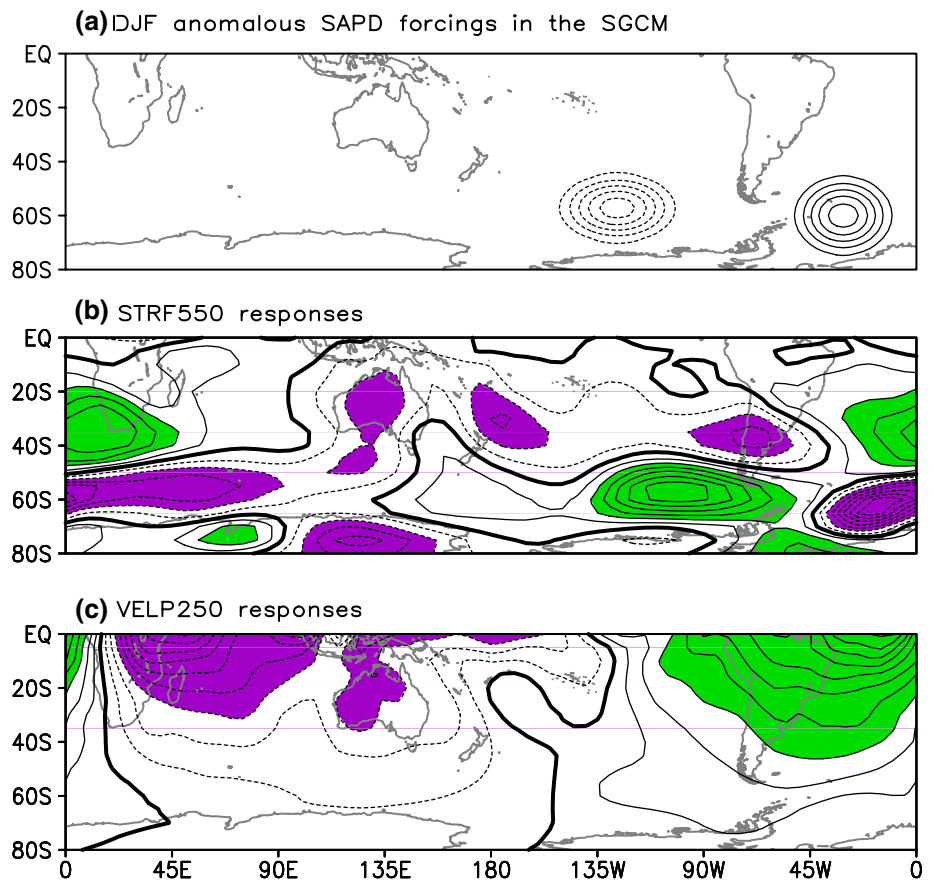


Fig. 11 **a** Vertically averaged anomalous heating rate for the ITCZI forcing run. The contour interval is 0.7 K day^{-1} . **b** 250 hPa geopotential height (Z250) responses. The contour interval is 6 gpm. The *green shadings* represent those with a positive response over 20 gpm,

blue below -20 gpm . The *bold contour* denotes zero. Contours with negative values are dashed for **a** and **b**. The zero contour for **a** is omitted

rapidly and may not sustain through the following winter, the SAPD SSTA around the Antarctic continent acts as a “recharger” and may “store” the SAM signals. It needs to be pointed out that based on Fig. 4, a tripole SSTA pattern exists in the Southern Hemisphere Indian Ocean. However, the mid-low latitude components of the tripole pattern (north of 40°S) are relatively weak and lack of persistence from ND through JF. Its high-latitude component is relatively obvious and exhibits some persistence. According to our numerical results with the SGCM (not shown), compared to the SAPD forcing, the SH Indian Ocean forcing is relatively weak as far as its influence to the ITCZ is concerned. Therefore, we did not focus on the tripole SSTA in this study.

A new mechanism on the cross-equatorial propagation of the SAM influence is proposed and may be summarized as follows. The SAPD SSTA pattern associated with the anomalous SAM excites a distinct Rossby wave train over the SH propagating from the Weddell sea towards the equator and affecting the variability of the Walker Circulation and the Pacific ITCZ. Subsequently, a distinguished atmospheric tele-connection pattern is induced and prevails over the NH mid-latitude region as a response to the anomalous ITCZ. Large areas of high pressure anomalies are triggered at upper troposphere over East Asia and centered over southern China, which favors less precipitation over East Asia, particularly southern China, and vice versa. Through such a process, the ND SAM may exert profound influences on the East Asian rainfall in the ensuing winter.

Our results suggest that the ND SAM may provide another predictability source for the NH climate. Nevertheless, some scientific issues remain. For instance, how could the SAM trigger the dipole SSTA around the Antarctic continent? The detailed process is not yet clear. Another interesting issue is that tropical SST proves to be able to affect the SAM variability (e.g., Ding et al. 2012; Ding and Steig 2013), how about vice versa? Since ENSO has a more direct effect on the Pacific ITCZ, what is the relative importance of the SAM and ENSO as far as the contribution to the ITCZ variability is concerned? These issues call for further investigations in future. In addition, due to lack of enough observational stations in the SH, monitoring efforts of the SAM should receive enhanced support.

Acknowledgments We appreciate the ECMWF for providing the re-analysis data. Zhiwei Wu is supported by the National Basic Research Program “973” (Grant No. 2013CB430202). This is publication No. 0002 of the Earth System Modeling Center (ESMC).

References

- Bretherton CS, Smith C, Wallace JM (1992) An inter-comparison of methods for finding coupled patterns in climate data. *J Clim* 5:541–560
- Cai W, Watterson IG (2002) Modes of interannual variability of the Southern Hemisphere circulation simulated by the CSIRO climate model. *J Clim* 15:1159–1174
- Cai W, Baines PG, Gordon HB (1999) Southern mid- to high-latitude variability, a zonal wavenumber 3 pattern, and the Antarctic Circumpolar Wave in the CSIRO coupled model. *J Clim* 12:3087–3104
- Cai W, Rensch P, Borlace S, Cowan T (2011) Does the Southern Annular Mode contribute to the persistence of the multidecadal drought over southwest Western Australia? *Geophys Res Lett* 38:L14712. doi:10.1029/2011GL047943
- Charney JG, Shukla J (1981) Predictability of monsoons. In: Light-hill J, Pearce RP (eds) *Monsoon dynamics*. Cambridge University Press, New York, pp 99–109
- Chen M, Xie P, Janowiak JE, Arkin PA (2002) Global land precipitation: a 50-yr monthly analysis based on gauge observations. *J Hydrometeorol* 3:249–266
- Dee DP, Uppala S, Simmons A et al (2011) The ERA–Interim reanalysis: configuration and performance of the data assimilation system. *Q J R Meteorol Soc* 137:553–597
- Ding QH, Steig EJ (2013) Temperature change on the Antarctic Peninsula linked to the Tropical Pacific. *J Clim* 26:7570–7585
- Ding QH, Steig EJ, Battisti DS, Wallace JM (2012) Influence of the tropics on the Southern Annular Mode. *J Clim* 25:6330–6348
- Feng J, Li JP, Li Y (2010) Is there a relationship between the SAM and southwest Western Australian winter rainfall? *J Clim* 23:6082–6089
- Gillett NP, Kell TD, Jones PD (2006) Regional climate impacts of the Southern Annular Mode. *Geophys Res Lett* 33(23):L23704. doi:10.1029/2006GL027721
- Hall NMJ (2000) A simple GCM based on dry dynamics and constant forcing. *J Atmos Sci* 57:1557–1572
- He JH, Lin H, Wu Z (2011) Another look at influences of the Madden–Julian Oscillation on the wintertime East Asian weather. *J Geophys Res* 116:D03109. doi:10.1029/2010JD014787
- Hendon H, Thompson DWJ, Wheeler MC (2007) Australian rainfall and surface temperature variations associated with the Southern Hemisphere annular mode. *J Clim* 20(11):2452–2467
- Hoskins BJ, Karoly DJ (1981) The steady linear response of a spherical atmosphere to thermal and orographic forcing. *J Atmos Sci* 38:1179–1196
- Hoskins BJ, Simmons AJ (1975) A multi-layer spectral model and the semi-implicit method. *Q J R Meteorol Soc* 101:637–655
- Kidson JW (1975) Eigenvector analysis of monthly mean surface data. *Mon Weather Rev* 103:182–186
- Kidson JW, Renwick JA, McGregor J (2009) Hemispheric-Scale Seasonality of the Southern Annular Mode and Impacts on the climate of New Zealand. *J Clim* 22:4759–4770
- L’Heureux ML, Thompson DWJ (2006) Observed relationships between El Niño–Southern Oscillation and the extratropical zonal-mean circulation. *J Clim* 19:276–287
- Li Y, Smith I (2009) A statistical downscaling model for Southern Australia winter rainfall. *J Clim* 22:1142–1158
- Li JP, Wu Z (2012) Importance of autumn Arctic sea ice to northern winter snowfall. *Proc Natl Acad Sci USA* 109. doi:10.1073/pnas.1205075109
- Li Y, Cai W, Campbell EP (2005) Statistical modeling of extreme rainfall in Southwest Australia. *J Clim* 18:852–863
- Lin H, Wu Z (2011) Contribution of the autumn Tibetan Plateau snow cover to seasonal prediction of North American winter temperature. *J Clim* 24:2801–2813
- Lorenz EN (1963) Deterministic nonperiodic flow. *J Atmos Sci* 20:130–141
- Marshall GJ (2003) Trends in the Southern Annular Mode from observations and reanalyses. *J Clim* 16:4134–4143
- Nan S, Li JP (2003) The relationship between the summer precipitation in the Yangtze River valley and the boreal spring Southern

- Hemisphere annular mode. *Geophys Res Lett* 30(24):2266. doi:[10.1029/2003GL018381](https://doi.org/10.1029/2003GL018381)
- Nan S, Li JP, Yuan X, Zhao P (2008) Boreal spring Southern Hemisphere annual mode, Indian Ocean SST and East Asian summer monsoon. *J Geophys Res* 114:D02103. doi:[10.1029/2008JD010045](https://doi.org/10.1029/2008JD010045)
- Rogers JR, Loon H (1982) Spatial variability of sea level pressure and 500 mb height anomalies over the Southern Hemisphere. *Mon Weather Rev* 110:1375–1392
- Shukla J (1998) Predictability in the midst of chaos: a scientific basis for climate forecasting. *Science* 282:728–731
- Smith TM, Reynolds RW, Peterson TC, Lawrimore J (2008) Improvements to NOAA's historical merged land–ocean surface temperature analysis (1880–2006). *J Clim* 21:2283–2296
- Sun C, Li JP (2012) Space–time spectral analysis of the Southern Hemisphere daily 500-hPa geopotential height. *Mon Weather Rev* 140:3844–3856
- Thomas RA, Webster PJ (1994) Horizontal and vertical structure of cross-equatorial wave propagation. *J Atmos Sci* 51:1417–1430
- Thompson DWJ, Wallace JM (2000a) Annular modes in the extratropical circulation. Part I: month-to-month variability. *J Clim* 13:1000–1016
- Thompson DWJ, Wallace JM (2000b) Annular modes in the extratropical circulation. Part I: trends. *J Clim* 13:1018–1036
- Trenberth KE, Stepaniak DP, Smith L (2005) Interannual variability of patterns of atmospheric mass distribution. *J Clim* 18:2812–2825
- Walker GT (1928) World weather. *Q J R Meteorol Soc* 54:79–87
- Wu ZW, Li J, Wang B, Liu X (2009a) Can the Southern Hemisphere annular mode affect China winter monsoon? *J Geophys Res* 114:D11107. doi:[10.1029/2008JD011501](https://doi.org/10.1029/2008JD011501)
- Wu ZW, Wang B, Li J, Jin FF (2009b) An empirical seasonal prediction model of the East Asian summer monsoon using ENSO and NAO. *J Geophys Res* 114:D18120. doi:[10.1029/2009JD011733](https://doi.org/10.1029/2009JD011733)
- Wu ZW, Li J, Jiang ZH, He JH (2011) Predictable climate dynamics of abnormal East Asian winter monsoon: once-in-a-century snowstorms in 2007/2008 winter. *Clim Dyn* 37:1661–1669
- Wu ZW, Li J, Jiang ZH, He JH, Zhu XY (2012) Possible effects of the North Atlantic Oscillation on the strengthening relationship between the East Asian summer monsoon and ENSO. *Int J Climatol* 32:794–800
- Xie P, Arkin PA (1997) Global precipitation: a 17-year monthly analysis based on gauge observations, satellite estimates, and numerical model outputs. *Bull Am Meteorol Soc* 78:2539–2558
- Xu HL, Li JP, Feng J, Mao JY (2013) The asymmetric relationship between the winter NAO and the precipitation in southwest China. *Acta Meteorol Sin* 70(6):1276–1291
- Yin S, Feng J, Li JP (2013) Influences of the preceding winter Northern Hemisphere annular mode on the spring extreme low temperature events in the north of eastern China. *Acta Meteorol Sin* 70(1):96–108
- Yuan XJ, Li CH (2008) Climate modes in southern high latitudes and their impacts on Antarctic sea ice. *J Geophys Res* 113(C6):C06S91. doi:[10.1029/2006JC004067](https://doi.org/10.1029/2006JC004067)
- Zheng F, Li JP (2012) Impact of preceding boreal winter southern hemisphere annular mode on spring precipitation over south China and related mechanism. *Chin J Geophys* 55(11):3542–3557